ECS Transactions, 23 (1) 61-68 (2009)
10.1149/1.3183702 © The Electrochemical Society

Three-Dimensional Plasma Etching Simulation using Advanced Ray Tracing and Level Set Techniques

O. Ertl and S. Selberherr

Institute for Microelectronics, TU Wien, Gußhausstr. 27-29/E360, A-1040 Wien, Austria

We present three-dimensional simulation techniques for plasma etching processes. Models based on Langmuir-type adsorption and on ballistic particle transport at feature scale can be efficiently solved in three dimensions. Surface coverages are self-consistently calculated. The local sputter rates of ions and the fluxes of neutrals are computed using modern ray tracing algorithms. In this way angle and energy dependent sputter yields or specular reflections of ions can be incorporated in a natural manner. For the time evolution of the surface we apply a recently developed fast multi-level-set framework. Our simulation techniques are demonstrated using a SF_6/O_2 plasma etching process model.

Introduction

In recent years various works on three-dimensional plasma etching simulation have been presented. However, most of them are not suitable to solve complex plasma etching models. The transport equations of more generalized models can not be solved in three dimensions by common surface integration techniques due to computational limitations. For simplification specular reflections of ions or higher order re-emissions of neutrals are often not fully incorporated (1, 2). A more promising approach is based on the Monte Carlo method. By simulating many particle trajectories the surface rates can be determined (3, 4). Compared to common techniques, where the particle transport equation is solved conventionally by integration over the surface, the Monte Carlo method allows the solution of more complex transport equations. We have recently shown that the application of modern ray tracing techniques leads to a well scaling algorithm suitable for large three-dimensional geometries (5). We present the application of these methods to more sophisticated physical models which are used to describe plasma etching processes.

Model

Typical plasma etching models assume ballistic transport of particles at feature-scale and Langmuir-type adsorption (6 - 9). As representative of these mathematically similar models we pick out the model given in (9) which describes silicon etching in SF_6/O_2 plasma. In the following we summarize the model. We also discuss the governing equations, in order to point up the difficulties of their solution, especially in three dimensions. However, for a detailed description of the model including full sets of parameters we refer to the original paper.

Particle Transport

The model incorporates three different particle types: Ions, etchants (fluorine), and inhibitors (oxygen). We assume that the arrival angle and energy distributions are known for all involved particle species at a plane P just above the surface as illustrated in Figure 1.

$$\Gamma^{\text{src}}(\mathbf{t},E)\,d\Omega dE = F^{\text{src}}\frac{\kappa+1}{2\pi}\left(\mathbf{t}\cdot\mathbf{n}_P\right)^{\kappa} f(E)\,d\Omega dE \qquad [1]$$

Here $\mathbf{n}_P$ is the normal of the plane P pointing towards the surface S of the structure. $\mathbf{t}$ is the incidence direction. F^{src} denotes the total arriving flux. The parameter κ is used to model the arrival angle distribution. For the narrow angular distribution of ions typically large values are used ($\kappa \approx 10^2 \ldots 10^3$). For neutral particle species usually $\kappa = 1$ is applied, which corresponds to a cosine-like angular distribution. The function $f(E)$ describes the energy distribution of particles, which can be obtained from plasma sheath calculations (10). The energy dependence in [1] is only taken into account for ions, since their energy has an impact on the sputter yield.

Ballistic transport from the plane P to the surface S is assumed (11). This is a good approximation, if the mean free path of particles is smaller than the typical feature size. Consequently, the particle flux arriving at the surface point $\mathbf{x}$ with direction $\mathbf{t}$ and energy E can be written as

$$\Gamma(\mathbf{x},\mathbf{t},E)d\Omega dE = \frac{-\mathbf{t}\cdot\mathbf{n}(\mathbf{x})}{\left\|\mathbf{x}-\mathbf{x}'\right\|^2}\cdot\begin{cases}\Gamma^{\text{src}}(\mathbf{t},E)dA'dE & \text{if } \mathbf{x}'\in P\\ \Gamma^{\text{re}}(\mathbf{x}',\mathbf{t},E)dA'dE & \text{if } \mathbf{x}'\in S\end{cases} \qquad \text{with } \mathbf{t}=\frac{\mathbf{x}-\mathbf{x}'}{\left\|\mathbf{x}-\mathbf{x}'\right\|}. \qquad [2]$$

Depending on its origin which can be either the plasma, represented by plane P, or the surface S itself due to re-emission, two cases are distinguished. $\mathbf{x}'$ is the closest point seen from point $\mathbf{x}$ in direction $-\mathbf{t}$ and which belongs to P or S.

Figure 1. The flux at a surface point $\mathbf{x}$ is composed of the direct flux from the source plane P and the indirect flux from the surface S itself due to re-emission.

Figure 2. Spatial subdivision accelerates the calculation of particle trajectories. Only a small number of boxes have to be traversed until the surface is reached.

The re-emitted flux Γ^{re} is related to the incidence flux distribution by the transmission probability $Q(\mathbf{n}(\mathbf{x});\mathbf{t},\mathbf{t}';E,E')$, which gives the probability that an incident particle with direction $\mathbf{t}'$ and energy E' is re-emitted into direction $\mathbf{t}$ with an energy E

$$\Gamma^{\text{re}}(\mathbf{x},\mathbf{t},E) = \iint Q(\mathbf{n}(\mathbf{x});\mathbf{t},\mathbf{t}';E,E')\Gamma(\mathbf{x},\mathbf{t}',E')d\Omega' dE'. \qquad [3]$$

To describe the diffusive re-emission of neutral particles with a sticking probability δ the transmission probability can be written as

$$Q(\mathbf{n}(\mathbf{x});\mathbf{t},\mathbf{t}') = (1-\delta)\frac{\mathbf{t}\cdot\mathbf{n}(\mathbf{x})}{\pi}. \qquad [4]$$

As already mentioned the energy distribution is neglected for neutral particles. The general formulation of the re-emission [3] also allows the description of specular-like scattering of ions. The applied angular and energy distributions of re-emitted ions as function of incidence angle and energy can be found in (8).

Surface Kinetics

For the description of the surface kinetics coverages $\theta_{\text{F}}(\mathbf{x})$ and $\theta_{\text{O}}(\mathbf{x})$ are introduced, which describe the fraction of surface sites covered with fluorine and oxygen, respectively. The corresponding balance equations can be written as

$$\begin{aligned} \sigma_{Si}\frac{d\theta_{\text{F}}}{dt} &= \gamma_{\text{F}}(1-\theta_{\text{F}}-\theta_{\text{O}})\int\Gamma_{\text{F}}(\mathbf{t})d\Omega - k\sigma_{\text{Si}}\theta_{\text{F}} - 2\theta_{\text{F}}\iint Y_{\text{Si}}(\mathbf{t},E)\Gamma_{\text{ion}}(\mathbf{t},E)d\Omega dE, \\ \sigma_{Si}\frac{d\theta_{\text{O}}}{dt} &= \gamma_{\text{O}}(1-\theta_{\text{F}}-\theta_{\text{O}})\int\Gamma_{\text{O}}(\mathbf{t})d\Omega - \beta\sigma_{\text{Si}}\theta_{\text{O}} - \theta_{\text{O}}\iint Y_{\text{O}}(\mathbf{t},E)\Gamma_{\text{ion}}(\mathbf{t},E)d\Omega dE. \end{aligned} \qquad [5]$$

Here σ_{Si} is the surface site density. The first terms describe the adsorption of neutrals, which is proportional to the corresponding arriving fluxes, the sticking probabilities $\gamma_{\text{F/O}}$, and the fraction of free surface sites ($1 - \theta_{\text{F}} - \theta_{\text{O}}$). The second term describes the loss of particles caused by chemical etching with rate k or by recombination with rate β, respectively. The third term describes the removal due to ion-enhanced etching or sputtering. Y_{Si} and Y_{O} are the ion-enhanced etching yield function and the O sputter yield function, respectively.

Usually the relaxation to equilibrium occurs on a much smaller time scale than geometric changes due to the advancing etch front. Hence, pseudo-steady-state conditions $\partial\theta/\partial t = 0$ can be assumed in [5], which leads to a system of linear equations with respect to the coverages. Consequently, the solution of this system leads to explicit expressions for the coverages. They can be directly calculated from the flux distributions. However, the flux distributions themselves depend on the coverages, since the effective sticking probabilities usually depend on the fraction of free surface sites. For example, the effective sticking probability in [4] is modeled by $\delta_{\text{F/O}} = \gamma_{\text{F/O}}(1-\theta_{\text{F}}-\theta_{\text{O}})$. This leads to a recursive problem, which has to be solved iteratively and which will be discussed later.

Once the flux distributions of all involved particle species are determined, the local etching rate

$$\mathrm{ER}=\frac{1}{\rho_{\mathrm{Si}}}\left(\frac{k\sigma_{\mathrm{Si}}\theta_{\mathrm{F}}}{4}+\iint Y_{\mathrm{p}}(\mathbf{t},E)\Gamma_{\mathrm{ion}}(\mathbf{t},E)d\Omega dE+\iint Y_{\mathrm{Si}}(\mathbf{t},E)\theta_{\mathrm{F}}\Gamma_{\mathrm{ion}}(\mathbf{t},E)d\Omega dE\right) \quad [6]$$

can be calculated as the sum of three contributions: Chemical etching, physical sputtering, and ion-enhanced etching. Here ρ_{Si} denotes the Si bulk density and Y_{p} is the physical sputter yield function.

Simulation Methods

In order to calculate the time evolution of the surface the local etch rates have to be determined at each time step by solving the system of equations [2], [5], and [6]. Then, the surface is moved according to these rates for the whole time step. If the time step is small, so that geometric changes do not have much influence on the local etch rates, this is a justified approach. In the following we briefly describe the methods which we use for calculating the movement of the surface and the local etch rates.

Level Set Method

For the surface evolution we use the level set method (12), which describes a moving boundary as zero level set of a continuous function. The solution of the level set equation

$$\frac{\partial\Phi}{\partial t}+\mathrm{V}(\mathbf{x})\left\|\nabla\Phi\right\|=0,\ \text{where}\ S=\left\{\mathbf{x}:\Phi(\mathbf{x})=0\right\} \quad [7]$$

gives the time evolution of the surface. Here $\Phi(\mathbf{x})$ denotes the level set function, and $\mathrm{V}(\mathbf{x})$ is the surface velocity field. Usually the level set equation is solved on a regular grid using finite difference schemes. The position of the surface is described with sub-grid accuracy and can be obtained by tri-linear interpolation within grid cells. Another advantage of the level set method is the inherent incorporation of topographic changes.

In its original formulation the level set function is stored and updated in time for all grid points of the simulation domain. The surface velocity field $\mathrm{V}(\mathbf{x})$ has to be determined by extrapolating the etch rates given on the surface. In summary, the calculation of the surface evolution scales with the simulation domain, not like the desired linear scaling with surface size.

Different methods have been developed to make the level set method more efficient. We have recently developed a fast level-set-framework (13) based on the sparse field level set method (14) and a hierarchical run-length-encoded level set data structure (15). There only a minimum set of grid points located close to the surface is stored and updated in time. In this way a linear scaling is obtained for the memory requirements as well as for the time evolution algorithm. In addition, the costly surface velocity extension can be avoided (5).

Ray Tracing

The calculation of the local flux distributions by solving [2] without any simplifications of the re-emission equation [3] is not reasonable in three dimensions by means of conventional surface integration techniques. To solve the particle transport in its general form, discretizations of the surface and of the solid angle are necessary. In

case of ions also an energy discretization is required. This leads to a huge number of unknowns resulting in large memory requirements. Additionally, the solution of the corresponding system of equations is very expensive.

Alternatively, a Monte Carlo method can be applied. By simulating millions of particle trajectories for each involved particle species, the integrals in [5] and [6], which are necessary for the calculation of the surface coverages and the etch rate can be directly computed. The particles are launched from a random position on the source plane P. The direction and the energy are also randomly generated under consideration of the corresponding distributions. If a particle hits the surface, it contributes to the values of the integrals according to the yield given by its incidence angle and energy. Then the particle is re-emitted following the transmission probability Q. The particle trajectory calculation is continued until the particle leaves the simulation domain or remains sticking on the surface. To enable the calculation of the local etch rates, tangential disks with predefined areas are set up for all surface points, for which the etch rates have to be calculated. Each particle hitting such a disk contributes to the local rate (5).

The main task during the Monte Carlo simulation is to find the first intersections of particle trajectories with the surface. Due to the assumed ballistic transport the particle trajectories are straight lines. Therefore, the problem is quite similar with ray tracing, a widely applied Monte Carlo technique in computer graphics. There, millions of light rays are computed to obtain a realistic picture of a three-dimensional scene.

Various algorithms have been developed to speed up ray tracing. A very popular technique is spatial subdivision as shown in Figure 2. The simulation domain is subsequently divided into boxes, until they do not contain any parts of the surface or their sizes equal that of grid cells. By sequentially traversing box by box the first intersection with the surface can be found very efficiently. The expected computational costs for the calculation of a particle trajectory is in the order of $O(\log N)$, where N denotes the surface size. The number of simulated particles has to scale with N to keep the number of incidences per unit area, and consequently the statistical accuracy constant. As result a total algorithmic complexity of order $O(N \log N)$ can be obtained. This is a much better scaling law as can be obtained by direct integration methods. For that reason ray tracing is a suitable method to calculate the particle transport for large three-dimensional simulations.

Simulation Algorithm

The whole simulation algorithm is composed of the surface evolution module based on the level set method, and the surface rate calculation module using the Monte Carlo method enhanced by ray tracing techniques. Figure 3 shows a simplified flow chart of our simulation algorithm. First the level set data structure is initialized according to the input geometry and initial values are assigned to the surface coverages. As already mentioned, the surface coverages depend on the flux distributions and vice versa, leading to a recursive problem which has to be solved iteratively. This is done by repeating the ray tracing and the calculation of the surface coverages until they converge. In practice, this iterative procedure is only applied at the very beginning to calculate the initial coverages. Later, the coverages of the previous time step are used for the etch rate calculation. Since the time increments are very small due to the Courant-Friedrichs-Lewy condition, which has to be fulfilled for the level set method, the geometric changes, and consequently also the changes of the coverages are small. In our simulations the maximum advancement of the surface within a time step is limited by 0.1 grid spacings.

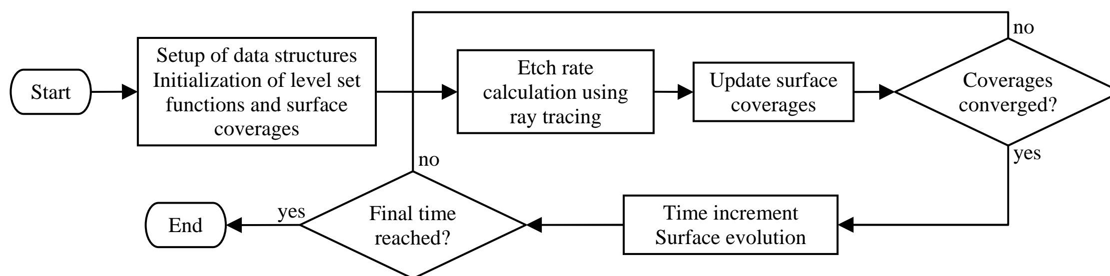

Figure 3. The flow chart of our simulation algorithm.

Simulation Results

To demonstrate our approach etching in SF_6/O_2 plasma is simulated. The initial structure is a silicon substrate covered by a 1.2µm thick SiO_2 mask layer with a circular tapered hole. The diameter is 0.35µm at the bottom and 0.4µm at the top. The geometry with two material regions is represented by two level sets resolved on a regular grid with lateral extensions 100 x 100 and a grid spacing of 20nm. Reflective boundary conditions are assumed in both lateral directions.

Figure 4 shows the level set representations of the profiles after 150s for different fluxes of oxygen and fluorine from the source. With increasing amount of oxygen the etched profile gets more directional. The oxygen covers the sidewalls and prevents them from corrosion. In our simulations mask etching is also incorporated. The applied multi-level-set technique allows an accurate description of multiple material regions with different surface rates (13).

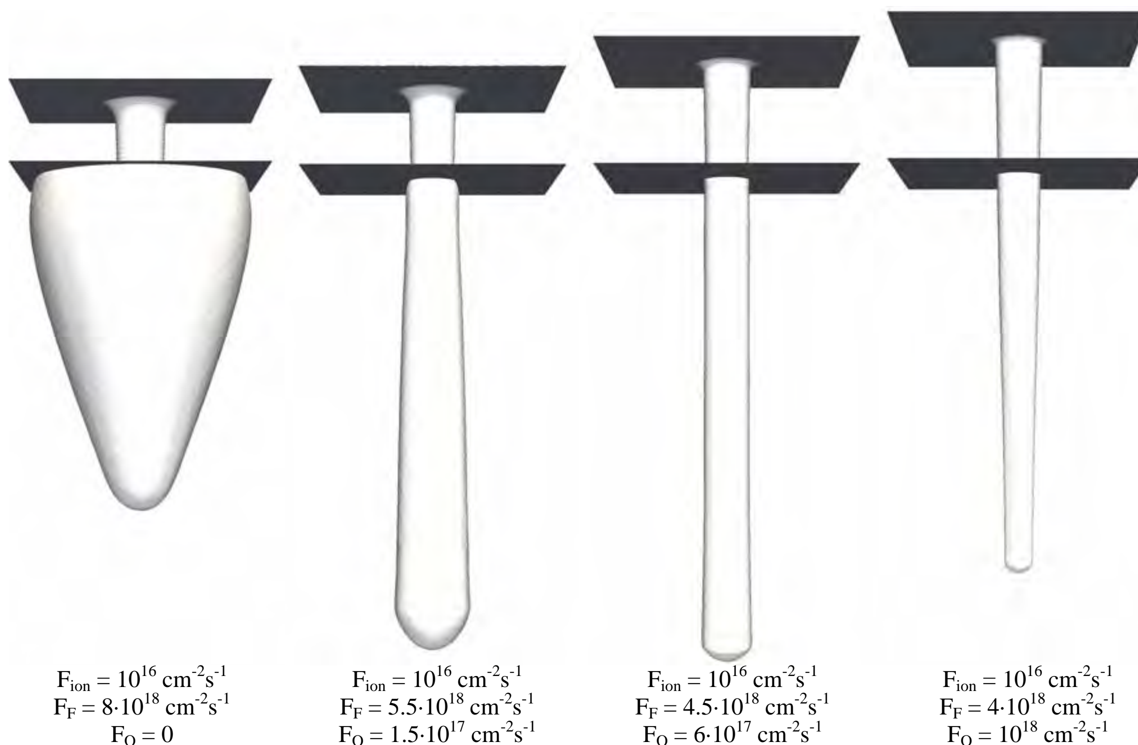

Figure 4. The final profiles after a process time of 150s for different fluxes of fluorine and oxygen. The two level sets which are used to represent the two material regions are shown. The mask corresponds to the region in between the two planes.

In each time step 5 million trajectories of each particle species are calculated. Due to spatial subdivision and the use of modern quad-core processors the calculation time of one time step could be reduced to less than 15s. About 2000 time steps are necessary to get the finale profiles, resulting in a total computation time of about 8h.

In a second example the three-dimensional capabilities of our simulator are demonstrated. The initial geometry is shown in Figure 5. The whole geometry is resolved on a grid with lateral extensions 200 x 200. Again reflective boundary conditions and a grid spacing of 20nm are used. The same process parameters are applied as for the third example in Figure 4. The level set representations of the profile after 25s, 50s, and 75s are shown in Figures 6 - 8. For this simulation, due to the larger domain size, 20 million particle trajectories of each species are calculated every time step. The full incorporation of specular reflections leads to micro-trenching at the trench bottom edges. Due to the same reason the bend and the end of the trench are etched deeper.

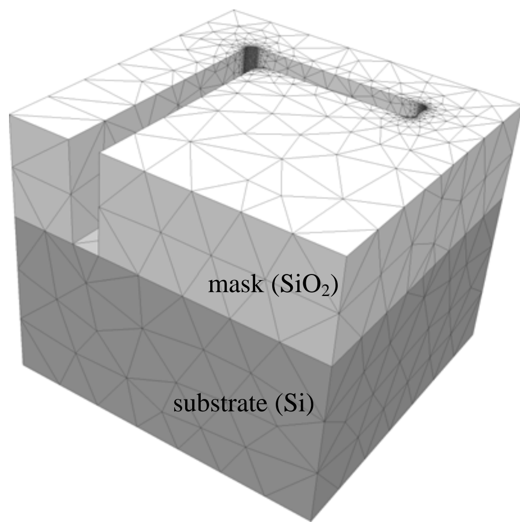

Figure 5. The initial geometry. The mask has a thickness of 1.2µm. The trench width is 0.35µm at the bottom and 0.4µm at the top.

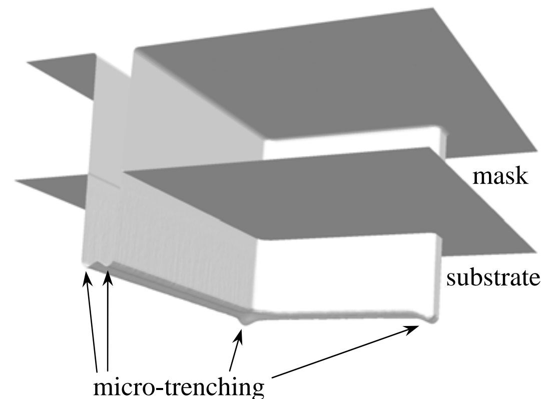

Figure 6. The profile after 25s. Micro-trenching as a result of specular reflections of ions can be clearly observed.

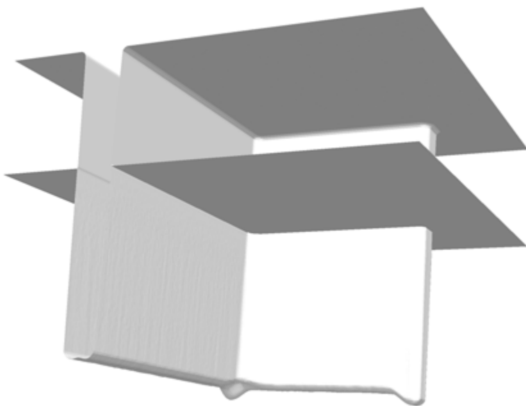

Figure 7. The profile after 50s.

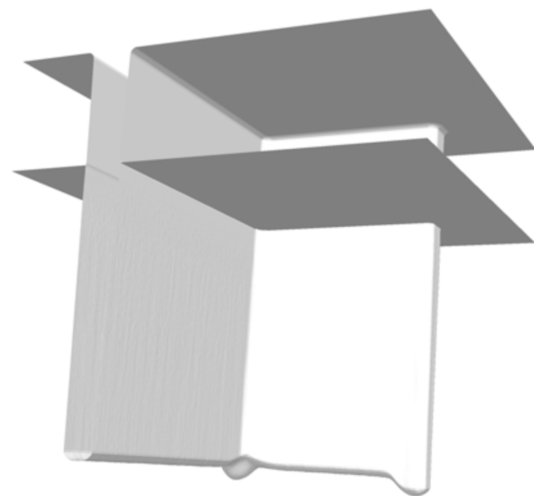

Figure 8. The profile after 75s.

Conclusion

We described simulation techniques which are able to solve complex plasma etching process models in three dimensions. Our ray tracing approach accelerated by spatial subdivision allows the efficient solution of the ballistic transport equations. Specular reflections as well as energy dependent and angle dependent sputter yields of ions can be incorporated. Coverages introduced within Langmuir-type adsorption models to describe the surface kinetics are self-consistently determined.

As demonstration we presented three-dimensional simulations of SF_6/O_2 plasma etching processes, where the influence of the particle fluxes on the final profile was investigated. The process was also applied to a non-symmetric trench structure, where three-dimensional effects could be observed, which were mainly caused by specular reflection of ions.

References

1. A. Hössinger, Z. Djuric, and A. Babayan, in Proc. *Intl. Conf. on Simulation of Semiconductor Processes and Devices (SISPAD)*, 53 (2007).
2. Y. H. Im, M. Bloomfield, C. Sukam, J. Tichy, T. Cale, and J. Seok, in Proc. *Intl. Conf. on Simulation of Semiconductor Processes and Devices (SISPAD)*, 307 (2003).
3. B. Radjenovic and J. K. Lee, in Proc. *17th Intl. Conf. on Phenomena in Ionized Gases (ICPIG)*, 17-142 (2005).
4. D. Kunder and E. Bär, *Microelectronic Engineering*, **85**, 992 (2008).
5. O. Ertl and S. Selberherr, *Microelectronic Engineering* (2009), DOI: 10.1016/j.mee.2009.05.011
6. S. Abdollahi-Alibeik, J. P. McVittie, K. C. Saraswat, V. Sukharev, and P. Schoenborn, *J. Vac. Sci. Technol. A*, **17** (5), 2485 (1999).
7. G. Kokkoris, A. Tserepi, A. G. Boudouvis, and E. Gogolides, *J. Vac. Sci. Technol. A*, **22** (4), 1896 (2004).
8. R. J. Belen, S. Gomez, M. Kiehlbauch, D. Cooperberg, and E. S. Aydil, *J. Vac. Sci. Technol. A*, **23** (1), 99 (2005).
9. R. J. Belen, S. Gomez, D. Cooperberg, M. Kiehlbauch, and E. S. Aydil, *J. Vac. Sci. Technol. A*, **23** (5), 1430 (2005).
10. E. Kawamura, V. Vahedi, M. A. Lieberman, and C. K. Birdsall, *Plasma Sources Sci. Technol.,* **8**, R45-R64 (1999).
11. T. S. Cale and G. B. Raupp, *J. Vac. Sci. Technol. B*, **8** (6), 1242 (1990).
12. S. Osher and J. A. Sethian, *J. Comput. Phys.*, **79** (1), 12 (1988).
13. O. Ertl and S. Selberherr, *Comput. Phys. Commun.* (2009), DOI: 10.1016/j.cpc.2009.02.002.
14. R. T. Whitaker, *J. Comput. Vision*, **29** (3), 203 (1998).
15. B. Houston, M. B. Nielsen, C. Batty, O. Nilsson, and K. Museth, *ACM Trans. Graph.*, **25** (1), 151 (2006).